



Supplement of

Oxidative potential apportionment of atmospheric PM₁: a new approach combining high-sensitive online analysers for chemical composition and offline OP measurement technique

Julie Camman et al.

Correspondence to: Benjamin Chazeau (benjamin.chazeau@psi.ch)

The copyright of individual parts of the supplement might differ from the article licence.

Supplementary Information

List of figures :

Figure S1. Percent of values above the MDL for each element measured with the Xact.

Figure S2. (a) Changes in $\Delta Q/Q_{exp}$, ΔUEV_{real} and ΔUEV_{noisy} for n-(n+1)-factor PMF_{metals} runs and **(b)** Q/Q_{exp} , UEV_{real} and UEV_{noisy} for PMF_{metals} runs from 1 to 8 factors. These PMF runs are performed for the WFP dataset. The box plots located in the blue dashed-line area represent the values for the finalized 6-factors bootstrap solution using the total metals dataset.

Figure S3. (a) Factors time series and **(b)** profiles from the PMF solution using the FDP dataset. The regional background factor profile was constrained with an a-value of 0.1.

Figure S4. Criteria scores for the 100 bootstrapped runs from the PMF_{metals}. Each graph represents one criterion for the different factors. The blue markers are for the factor criterion scores and the black markers represent the second highest scores attributed to one of the remaining factors.

Figure S5. (a) NO_x, SO₂ and O₃ concentration and **(b)** wind speed and direction during OP measurement period.

Figure S6. (a) Comparison between time series of PM₁ measured by FIDAS and time series of particulate fraction reconstituted by the sum of chemical components ($r_s = 0.47$, $p < 0.001$). **(b)** Contribution to PM₁ of chemical components (%) measured from 11th July 2018 to 25th July 2018 (included firework episode, n=91) by ToF-ACSM, Xact and aethalometer online analyzers.

Figure S7. (a) Average mass spectra profiles, **(b)** time-series, **(c)** pie chart contributions and **(d)** mean diurnal cycles (solid lines and error bars indicate the standard deviation) for the 5 factors from the PMF_{organics} solution.

Figure S8. (a) Pie chart contributions and **(b)** average diurnal profiles of factors from the PMF_{metals} analysis. For the diurnal plots the red dots correspond to the mean, the bands are the median, the bottom and top of the boxes represent the 25th and 75th percentile respectively, and the ends of the whiskers are for the 10th and 90th percentiles.

Figure S9. NWR plots for the different factors from the PMF_{metals} analysis.

Figure S10. Probability density function of scaled residuals for the standalone ACSM_OA, ACSM, AE33 and Xact datasets.

Figure S11. Box plots of dust resuspension factor concentrations for different relative humidity (RH) bins in %. The concentrations are enhanced under low RH conditions. The blue diamonds are the mean, the bars inside the boxes the median, the bottom and top of the boxes are the 25th and 75th percentile, respectively, and the ends of the whiskers are the 10th and 90th percentiles.

Figure S12. Criteria scores for the a-values sensitivity test runs from the PMF_{PM1}. Each graph represents one criterion per factor. The grey markers are the unselected runs, the blue markers are the selected runs for the related factor and the green markers are the effectively chosen runs.

Figure S13. Number of accepted solutions based on the PMF_{PM1} criteria list for the different a-values explored in the sensitivity test. A-values associated to the greatest number of validated solutions were

39 chosen for the bootstrap PMF runs (i.e. 0.4 for biomass burning, 0.1 for cooking and 0.05 for industrial
40 constrained profiles).

41 **Figure S14.** Relative contributions of PM₁ factors profiles and unexplained variations from the PMF_{PM1}
42 analysis.

43 **Figure S15.** Comparison between the industrial metals profile from our study and ICP-MS profiles for
44 the PM_{2.5} fraction in the industrial area of Fos-sur-mer (Sylvestre et al., 2017). Complex n°1 is a cast iron
45 converter complex, complex n°2 is a ore iron converter complex, complex n°3 is a blast furnace slag
46 storage and complex n°4 is an ore terminal.

47 **Figure S16.** Average diurnal profiles for SO₂, Sh-IndOA and the sum of industrial and shipping factors
48 from the PMF_{metals}.

49 **Figure S17.** NWR plots for each factor of the PMF_{PM1} analysis.

50 **Figure S18.** Average factor profiles for the PMF_{PM1} solution using OA factors, ACSM inorganic species,
51 BC and metals as inputs. The sticks represent the normalized contribution of the variable to the factor
52 (left axis) and markers show the normalized factor contribution to each variable (right axis).

53 **Figure S19.** Factor profiles from the PMF solution using organic m/z fragments, ACSM inorganic
54 species, BC and metals as inputs. The sticks represent the normalized contribution of the variable to
55 the factor (left axis) and markers show the normalized factor contribution to each variable (right axis).

56 **Figure S20.** Residuals values of WLS models for **(a)** OP_{AA} and **(b)** OP_{DTT}. An outlier point (07/19/2018
57 03:00) was withdrawn to ensure homoscedasticity of residuals values.

58 **Figure S21.** Mean contribution of the sources identified by PMF_{PM1} over the OP sampling campaign
59 (n = 86) to **(a)** OP_{AA}, **(b)** OP_{DTT}, **(c)** PM₁. Error bars represents the standard deviation of the data
60 distribution.

61

62 *List of tables :*

63 **Table S1.** List of elements measured with the Xact, their respective MDLs and the percent of
64 measurements above the MDL.

65 **Table S2.** Summary of statistics for the different PMF tests carried out on the WFP datasets of metals.
66 18 downweight conditions were tested for the PMF inputs. The matrix including a S2N downweight
67 and errors below MDLs downweighted with $\alpha_i = 2 \times r_{p95}$ (test n°12) was selected as final inputs.

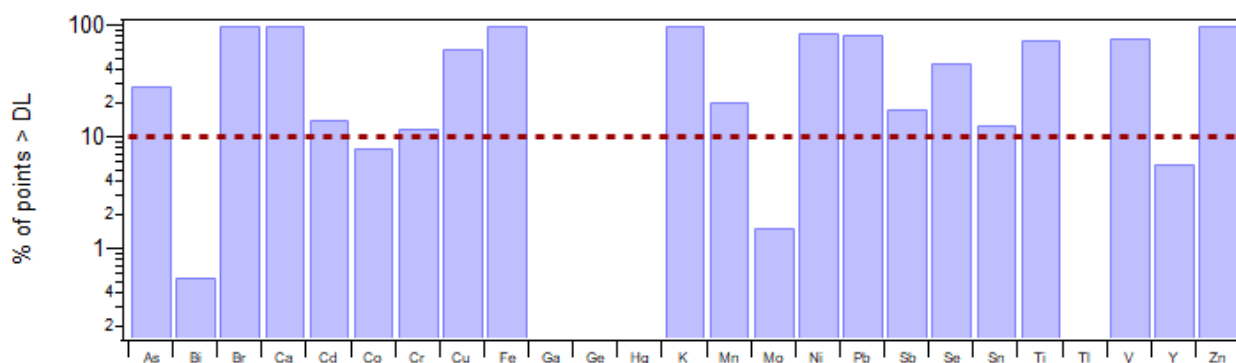
68 **Table S3.** Intrinsic OP_{AA} and OP_{DTT} (OP_m) provided by weighted robust linear regression with an M-
69 estimator expressed in $nmol.min^{-1}.\mu g^{-1}$ of sources provided by **(a)** $PMF_{organics}$ (scenario 1) and **(b)**
70 PMF_{metals} (scenario 2) over the OP sampling campaign ($n = 90$). Values are the mean \pm standard deviation
71 from bootstraps runs for both OP assays. The model parameters $R^2_{adjusted}$ and Pearson's correlation
72 between model OP and observed OP are mentioned on the right.

73 **Table S4.** Factors identification for the PMF_{PMI} analyses between 5 and 12 factors. The green cells
74 represent the base case identification for the related factors. The remaining undefined factors for each
75 solution corresponded to mixed profiles not attributed to a specific source. The red squares are the base
76 cases used as reference profile constraints.

77 **Table S5.** R^2 and slope values for the comparison of the PMF_{PMI} (OA factors + metals + ions + BC) factors
78 with PMF^2 factors. The relative contributions are also represented (in %).

79 **Table S6.** Pearson's correlation coefficients between OP_{VAA} and OP_{VDTT} to the PM sources identified by
80 PMF_{PMI} model.

81



82

83 **Figure S1.** Percent of values above the MDL for each element measured with the Xact.

84

85

86

Elements	MDL (ng.m ⁻³)	Values > MDL (%)
As	0.11	29.3
Bi	0.23	0.6
Br	0.18	99.8
Ca	0.52	99.5
Cd	4.4	14.4
Co	0.24	8.1
Cr	0.2	12.0
Cu	0.14	63.3
Fe	0.3	100
Ga	0.1	0
Ge	0.1	0
Hg	0.21	0.2
K	2	100
Mn	0.25	20.6
Mo	0.84	1.5
Ni	0.17	86.6
Pb	0.22	84.8
Sb	9	18.0
Se	0.14	46.4
Sn	7.1	12.8
Ti	0.28	76.0
Tl	0.2	0
V	0.21	76.7
Y	0.48	5.8
Zn	0.12	100

87 **Table S1.** List of elements measured with the Xact, their respective MDLs and the percent of
 88 measurements above the MDL.

89

90 **Sect. S1: Error matrix downweights for PMF_{metals}**

91 Polissar et al. (1998) (Polissar et al., 1998a) first introduced an uncertainty of $5/6 \times MDL$ for data below
92 MDL (set to $MDL/2$). The purpose was to provide relative errors for these values 2 to 5 times greater
93 than the maximum relative errors of the data exceeding the MDLs. Here, several uncertainties values
94 were tested for data below MDL by conducted a panel of PMF runs with 2 to 8 factors. The errors were
95 calculated by applying a downweight coefficient (α) to the previous formula from Polissar et al. (1998)
96 (Polissar et al., 1998a):

97
$$\sigma_{i,j} = \alpha \times \frac{5}{6} MDL_i \text{ if } x_{i,j} < MDL_i \quad (S1)$$

98 For all the elements i , α was set to 6, 10 and 14 in order to obtain a ratio of 2, 3.5 and 5, respectively,
99 with the maximum relative error found in the dataset, i.e. 476% for Sn (the value corresponds to the 95th
100 percentile instead of the max value to avoid outlier effects). Another test consisted in applying a
101 dependant α based on the maximum relative error (95th percentile) for each element i (r_{p95}):

102
$$\alpha_i = 2 \times r_{p95} \quad (S2)$$

103 Where 2 was used to determine the same ratio between the relative error of data below the MDLs from
104 Polissar et al. (1998) equation (167 %, considering the $\frac{5}{6}MDL/\frac{1}{2}MDL$ calculation) and the maximum
105 relative error for the data greater than the MDLs (50%) found in Polissar et al. (1998) (Polissar et al.,
106 1998a) dataset. A last test was performed with $\alpha=1$ (i.e. no downweight) for the comparison. Each PMF
107 analysis was also conducted with and without 1/S2N downweight (Visser et al., 2015). The tests were
108 performed on the WFP dataset and the results were synthetized in Table S2. Here we focus on the 5F-
109 solutions results as they resolved unmixed factors and represented a statistically relevant number of
110 factor (see section 2.4.2 in the main text).

111 For all PMF solutions, applying the 1/S2N downweight provided lower scaled residuals as shown by
112 the narrower width of fits. The solutions with $\alpha=1$ (i.e. no errors downweight for data $<MDLs$) were
113 discarded due to less satisfactory mass reconstructions and residuals and higher average unexplained
114 variations. The unexplained variation is a dimensionless quantity which indicates how much variation
115 (in time or in each variable) is not explained by the factors (Canonaco et al., 2013). Thus, the unexplained
116 variation of the i^{th} point for the factor k^{th} is:

117
$$UEV_{ik} = \frac{\sum_{j=1}^m (|e_{ij}|/\sigma_{ij})}{\sum_{j=1}^m ((\sum_{k=1}^p |g_{ik} \cdot f_{kj}| + e_{ij})/\sigma_{ij})} \quad (S3)$$

118 UEV is further calculated for data with $S2N > 2$ (UEV_{real}) or for noisy data (UEV_{noisy}).

119 The remaining tests gave comparable explained variations, mass reconstitutions and residuals. The
 120 uncertainties calculated with $\alpha_i = 2 \times r_{p95}$ (test n°12 in Table S2) were finally selected as error inputs
 121 for the data below the MDLs since this solutions resolved 5 unmixed factors with the best mean and
 122 median diurnal patterns for each identified source.

123

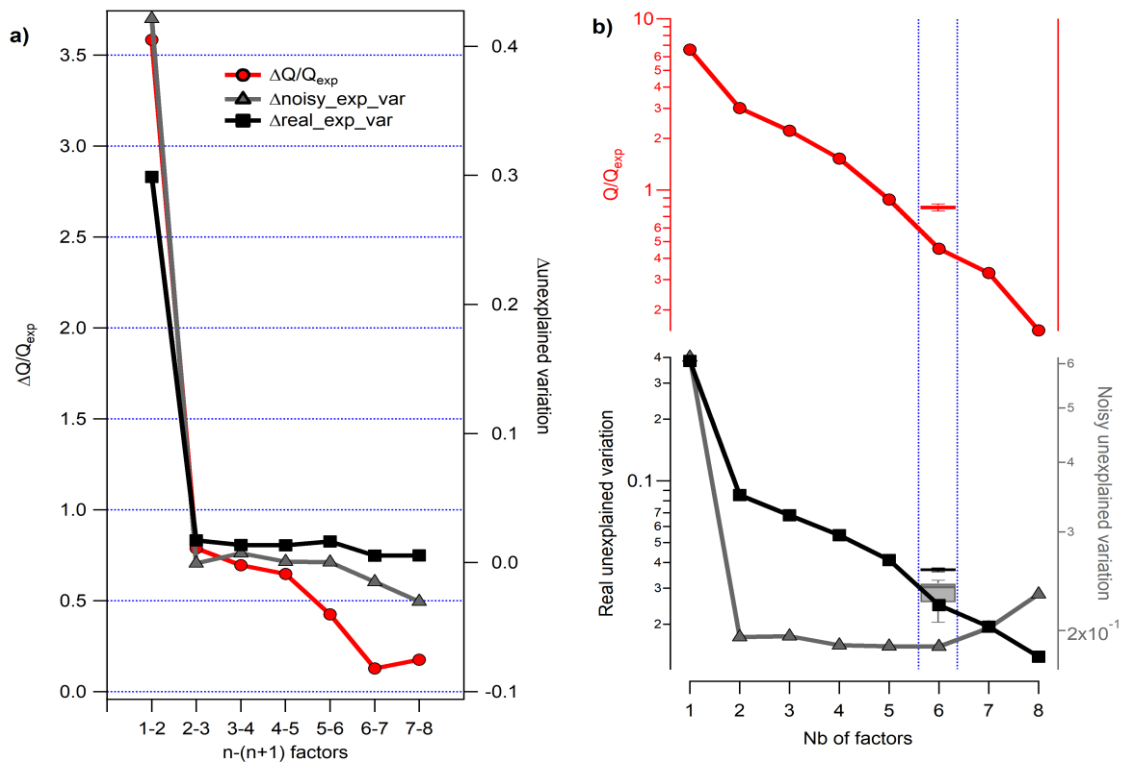
Tests	N°	Unexplained Variations			$\Sigma_{\text{factors vs } \Sigma_{\text{metals}}}$		Sc residuals	
		F5 EV_Noise	F5 EV_Real	F5 EV_Sum	F5 Slope	F5 R ²	F5 center	F5 width
noDW_noS2N	1	0.215	0.049	0.264	0.987	0.958	0.094	0.337
noDW_S2N	2	0.221	0.042	0.263	0.987	0.959	0.059	0.201
DW6_ALL_noS2N	3	0.187	0.048	0.235	0.989	0.973	-0.023	0.137
DW6_ALL_S2N	4	0.203	0.033	0.236	1.004	0.985	-0.002	0.014
DW6_SPEC_noS2N	5	0.187	0.041	0.228	1.000	0.979	-0.010	0.089
DW6_SPEC_S2N	6	0.203	0.033	0.236	1.003	0.986	-0.002	0.014
DW10_ALL_noS2N	7	0.187	0.040	0.227	1.010	0.993	-0.020	0.074
DW10_ALL_S2N	8	0.201	0.033	0.234	1.015	1.000	-0.002	0.005
DW10_SPEC_noS2N	9	0.187	0.040	0.227	1.010	0.993	-0.020	0.073
DW10_SPEC_S2N	10	0.201	0.033	0.234	1.014	1.000	-0.002	0.005
Roll_DW_ALL_noS2N	11	0.188	0.041	0.229	1.007	0.988	-0.013	0.091
Roll_DW_ALL_S2N	12	0.203	0.034	0.237	1.010	0.995	-0.001	0.005
Roll_DW_SPEC_noS2N	13	0.187	0.041	0.228	1.006	0.988	-0.013	0.091
Roll_DW_SPEC_S2N	14	0.203	0.034	0.237	1.011	0.995	-0.002	0.011
DW14_ALL_noS2N	15	0.189	0.040	0.229	1.016	1.000	-0.023	0.063
DW14_ALL_S2N	16	0.204	0.032	0.236	1.017	0.999	-0.002	0.005
DW14_SPEC_noS2N	17	0.189	0.040	0.229	1.016	1.000	-0.023	0.063
DW14_SPEC_S2N	18	0.203	0.033	0.236	1.023	1.000	-0.001	0.003

124 **Table S2.** Summary of statistics for the different PMF tests carried out on the WFP datasets of metals.
 125 18 downweight conditions were tested for the PMF inputs. The matrix including a S2N downweight
 126 and errors below MDLs downweighted with $\alpha_i = 2 \times r_{p95}$ (test n°12) was selected as final inputs.

127

128

129

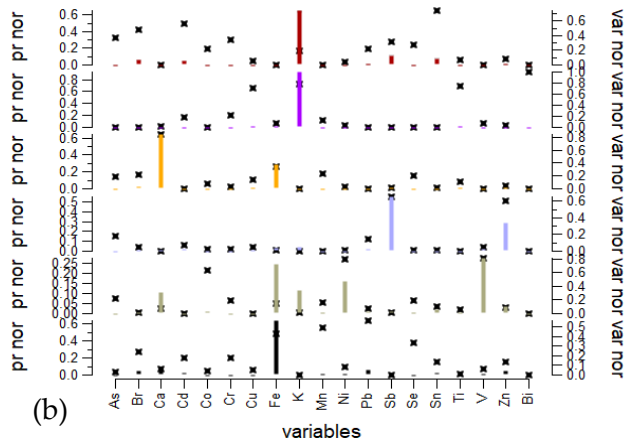
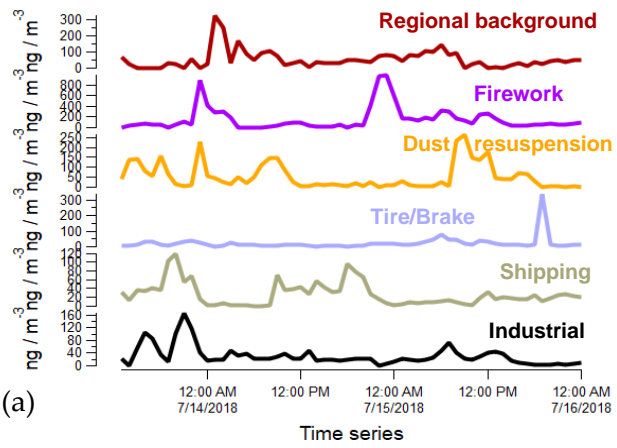


130

131 **Figure S2. (a)** Changes in $\Delta Q/Q_{exp}$, ΔUEV_{real} and ΔUEV_{noisy} for $n-(n+1)$ -factor PMF_{metals} runs and **(b)**
 132 Q/Q_{exp} , UEV_{real} and UEV_{noisy} for PMF_{metals} runs from 1 to 8 factors. These PMF runs are performed for the
 133 WFP dataset. The box plots located in the blue dashed-line area represent the values for the finalized 6-
 134 factors bootstrap solution using the total metals dataset.

135

136



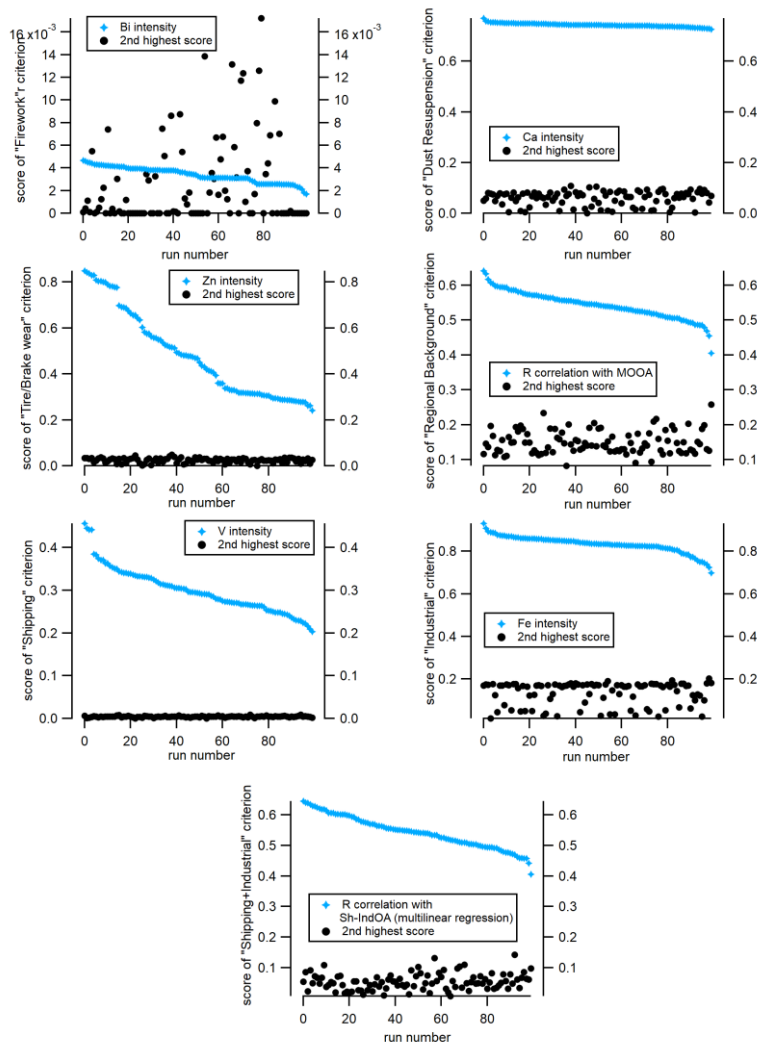
137

138 **Figure S3. (a)** Factors time series and **(b)** profiles from the PMF solution using the FDP dataset. The
 139 regional background factor profile was constrained with an a-value of 0.1.

140

141 **Sect. S2: Criteria selection for PMF_{metals}**

142 A first type of criterion was the use of the dominant element in the related factor. Thus, the Bi, Ca, Zn,
143 V and Fe intensity in profiles were monitored for the Firework, Dust resuspension, Tire/brake wear,
144 Shipping and Industrial factors, respectively. Then we inspected the r Pearson correlation with MOOA
145 for the regional background. A last criterion was the r Pearson correlation based on the multilinear
146 regression analysis of both shipping and industrial vs SO₂ concentrations. The statistical acceptance of
147 a run was based on the comparison between the criterion scores of a factor and the second highest scores
148 from the remaining factors (Fig. S4). For all criteria the second highest scores were much lower in every
149 run, with some rejected scores for the firework criterion. In total 25% of the runs were discarded based
150 on this criterion, and the remaining runs were averaged into a unique solution.



151
152 **Figure S4.** Criteria scores for the 100 bootstrapped runs from the PMF_{metals}. Each graph represents one
153 criterion for the different factors. The blue markers are for the factor criterion scores and the black
154 markers represent the second highest scores attributed to one of the remaining factors.

155

156 **Scenario and regression model selection for OP apportionment**

157 Three scenarii in the construction of the matrix of the source factors contribution to PM mass identified
158 by the three PMF have been considered to make the best use of the results from the different PMF:

- 159 • Scenario 1: OP apportionment from independent variables with the OA factors from PMF_{organics} (83
160 observations), following:

$$161 \quad OP = G \times \beta_g + \varepsilon \quad (S4)$$

- 162 • Scenario 2: OP apportionment from independent variables considering only the metals factors from
163 PMF_{metals} (90 observations), following:

$$164 \quad OP = H \times \beta_h + \varepsilon \quad (S5)$$

- 165 • Scenario 3: OP apportionment taking as independent variables PM₁ factors from PMF_{PM1} (78
166 observations), following (Eq. S6). In this configuration, the firework episode has been removed from
167 the data as the sources from the PMF_{PM1} analysis have been determined without including the
168 firework metal factor.

$$169 \quad OP = I \times \beta_i + \varepsilon \quad (S6)$$

170 In (Eq. S4, S5, S6), OP vector (p×1) is the observed OP expressed in volume unit, G matrix (g × (p+1)) of
171 g sources (plus the intercept) is determined by PMF_{organics}, H matrix (h × (p+1)) of h sources (plus the
172 intercept) is determined by PMF_{metal}, I matrix (i × (p+1)) of i sources (plus the intercept) is determined
173 by PMF_{PM1}, and ε vector (p×1) is the discrepancy between the model and the observations.

174 Three models were tested for the three scenarii (e.g. 9 solutions): weighted least squares linear
175 regression (WLS), weighted robust multiple linear regression with an iterative M-estimator, and partial
176 least square regression (PLS):

- 177 • WLS regression considers the uncertainties σ of the OP measurements by minimizing the weighted
178 sum of squares function (WSS):

$$179 \quad WSS(\beta) = \sum_{i=1}^p w_i (y_i - \sum_{j=1}^n x_{ij} * \beta_j)^2, \quad w_i = \frac{1}{\sigma_i} \quad (S7)$$

180 where y_i is the measured OP (p observations), x_{ij} is the values of n sources determined by PMF and σ_i
181 is the OP uncertainties. This method already used in this purpose in previous studies (Borlaza et al.,
182 2021; Weber et al., 2018, 2021) well suited to extracting maximum information from small data sets.
183 Ordinary Least Squares (OLS) is a simple special case of WLS where σ = 1.

- 184 • Linear weighted robust regression methods by M-estimator minimizes the function ρ:

$$185 \quad M(\beta) = \sum_{i=1}^p \rho(w_i (y_i - \sum_{j=1}^n x_{ij} * \beta_j)) \quad (S8)$$

$$\rho_k(x) = \begin{cases} \frac{x^2}{2} & \text{if } |x| < k = 1.5 \\ k \left(|x| - \frac{k}{2} \right) & \text{if } |x| \geq k = 1.5 \end{cases} \quad (\text{S9})$$

187 Based on similar work in Grange et al. (2022), Huber's function ρ and $k=1.5$ were used in this study.
 188 This technique is adapted to data sets presenting particular events(de Menezes et al., 2021), as fireworks
 189 on 13th and 14th of July -National day of France- in our data set. Indeed, the regression by successive
 190 iterations implies lower weights on outliers, which tends to underestimate these points. We can note
 191 WLS regression is a simple special case where $\rho(x) = x^2$.

- 192 • PLS regression is a method that reduces the predictors to a smaller set of uncorrelated components
 193 and performs least squares regression on these components. It is especially useful when dependent
 194 variables are highly correlated. Moreover, unlike multiple regression, PLS does not imply that the
 195 predictors are fixed but can be measured with error, making PLS more robust to measurement
 196 uncertainties.

197

198 **OP apportionment from PMF_{organics} (scenario 1) and PMF_{metals} (scenario 2)**

199 M-estimator inversion model's results issued from PMF_{organics} (scenario 1) and PMF_{metals} (scenario 2)
 200 alone are respectively presented in Table S 3a. and Table S 3b. β coefficients (i.e intrinsic OP, see 2.5)
 201 obtained by M-estimator model from PMF_{metals} display values an order of magnitude higher than those
 202 issued from PMF_{organics} inversion. This stress the importance of metals in OP apportionment, for both
 203 assays. Among the organic factors, only the Sh-IndOA factor seems to be slightly more sensitive to
 204 OP_{VDTT}. The Firework factor constrains a significant part of the data, implying a fairly high Pearson's
 205 correlation coefficient between OP_{model} and OP_{observed}. Nevertheless, R^2_{adjusted} of both M-estimator
 206 inversion models in scenario 1 (only organic fraction of PM is considered) indicated that the percentage
 207 of OP_{AA} and OP_{DDT} variance explained by the models is weak. On the other hand, several studies
 208 highlighted the role of Secondary Organic Aerosol (SOA) in the oxidative potential indicating that
 209 apportion OP from the metallic data alone is an incomplete step. Finally, the bootstrap method (see 2.5)
 210 applied to the four M-estimator models in these two scenarii did not achieve their convergence and are
 211 therefore not robust. Overall, this confirms that OP reflects the overall redox-activity of wide spectra of
 212 multispecies of organics, inorganics, metals and synergistic/antagonistic reactions between these
 213 compounds, and assess the importance to consider all these chemical compounds in the OP
 214 apportionment process.

(a)

	Intercept	COA	HOA	LOOA	MOOA	Sh-IndOA	R^2 adjusted	r (OP _{observed} /OP _{model})
OP _{AA}	0.19 ± 0.04	0.00 ± 0.02	0.02 ± 0.01	0.10 ± 0.04	0.04 ± 0.02	0.24 ± 0.09	0.27	0.48***
OP _{DTT}	0.38 ± 0.10	-0.04 ± 0.10	-0.12 ± 0.05	0.23 ± 0.04	0.1 ± 0.07	1.41 ± 0.15	0.41	0.51***

(b)

	Intercept	Firework	Industrial	Regional background	Shipping	Tire brake	R^2 adjusted	r (OP _{observed} /OP _{model})
OP _{AA}	0.36 ± 0.02	1.57 ± 0.16	3.21 ± 0.42	2.30 ± 0.33	-0.74 ± 0.68	n.c.	0.66	0.73***
OP _{DTT}	0.61 ± 0.12	4.17 ± 0.83	-1.24 ± 1.64	7.11 ± 2.30	17.0 ± 5.3	6.0 ± 4.60	0.38	0.61***

215

216

Table S3. Intrinsic OP_{AA} and OP_{DTT} (OP_m) provided by weighted robust linear regression with an M-estimator expressed in nmol.min⁻¹.µg⁻¹ of sources provided by (a) PMF_{organics} (scenario 1) and (b) PMF_{metals} (scenario 2) over the OP sampling campaign (n = 90). Values are the mean ± standard deviation from bootstraps runs for both OP assays. The model parameters R²_{adjusted} and Pearson's correlation between model OP and observed OP are mentioned on the right.

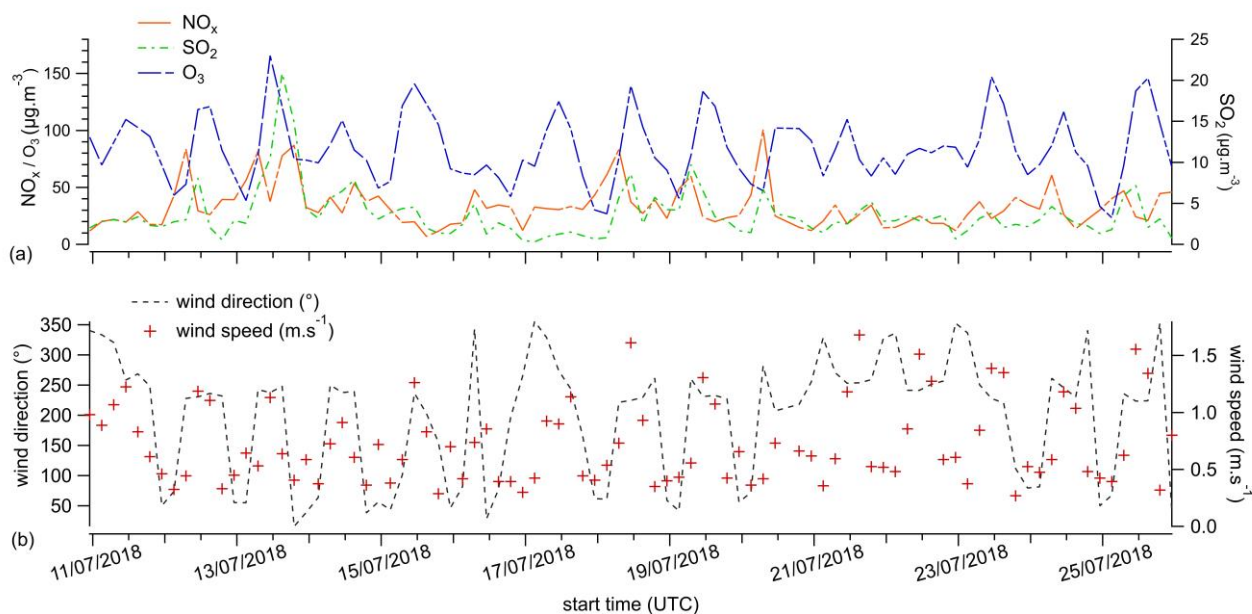
217

218

219

220

221

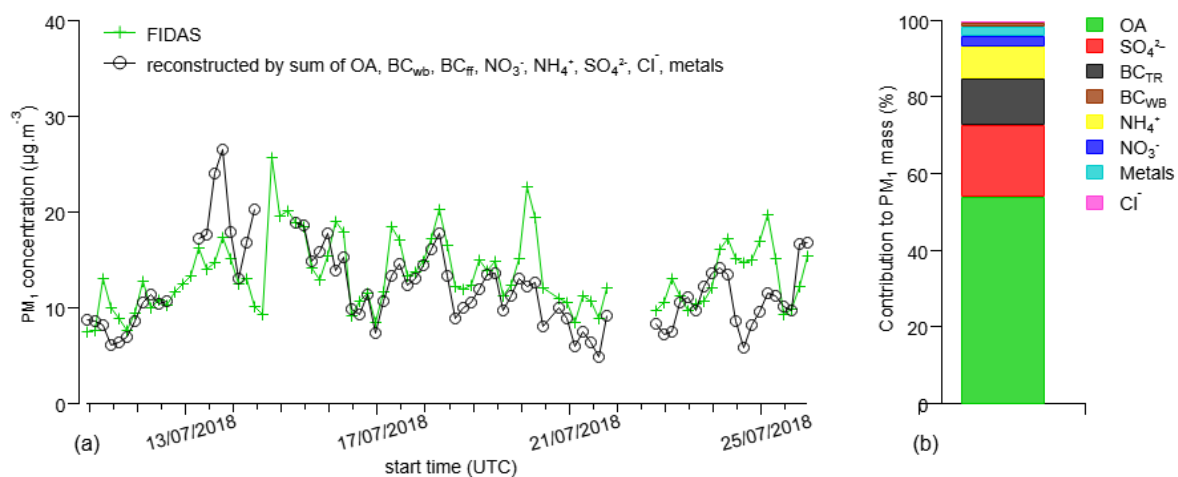


222

Figure S5. (a) NO_x, SO₂ and O₃ concentration and (b) wind speed and direction during OP measurement period.

224

225



226

227 **Figure S6. (a)** Comparison between time series of PM₁ measured by FIDAS and time series of particulate
 228 fraction reconstituted by the sum of chemical components ($r_s = 0.47$, $p < 0.001$); **(b)** Contribution to PM₁
 229 of chemical components (%) measured from 11th July 2018 to 25th July 2018 (included firework episode,
 230 $n=91$) by ToF-ACSM, Xact and aethalometer online analyzers.

231

232

233

234

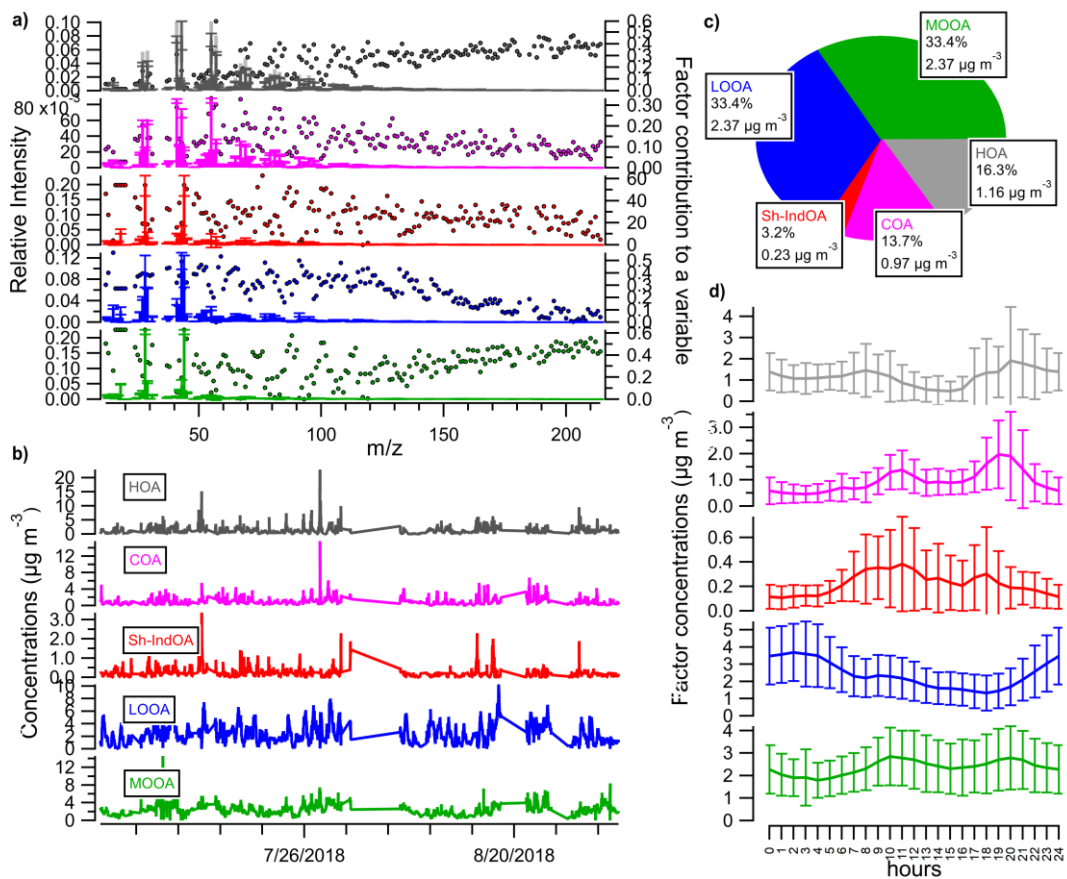
235

236

237

238

239

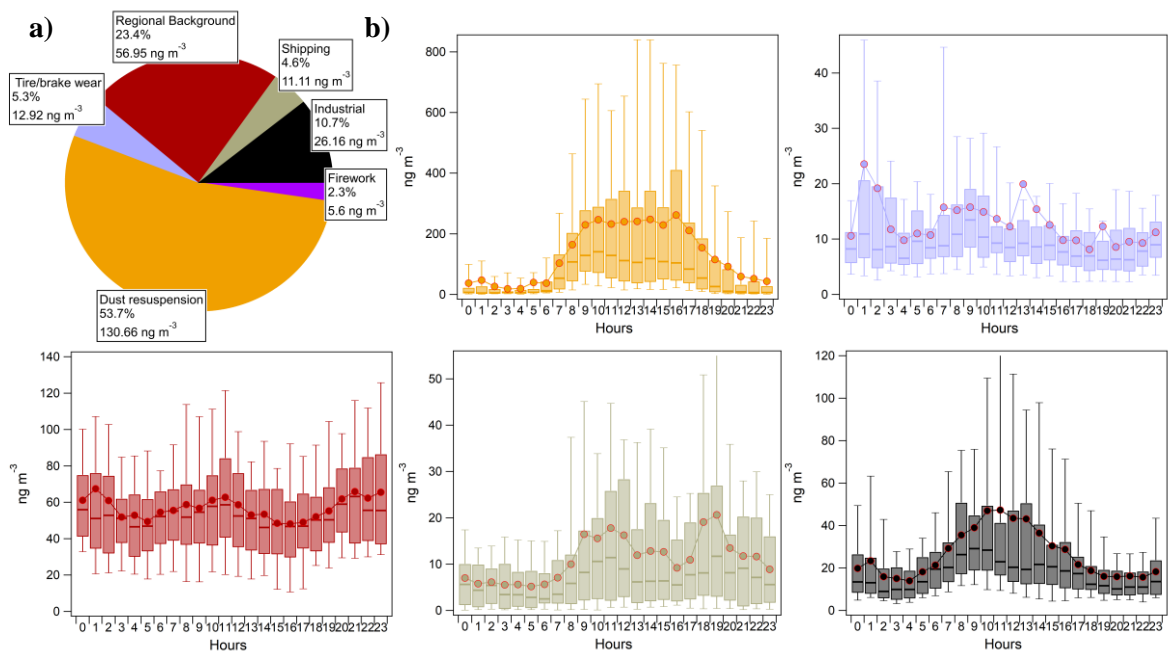


240

241 **Figure S7. (a)** Average mass spectra profiles, **(b)** time-series, **(c)** pie chart contributions and **(d)** mean
 242 diurnal cycles (solid lines and error bars indicate the standard deviation) for the 5 factors from the
 243 PMF_{organics} solution.

244

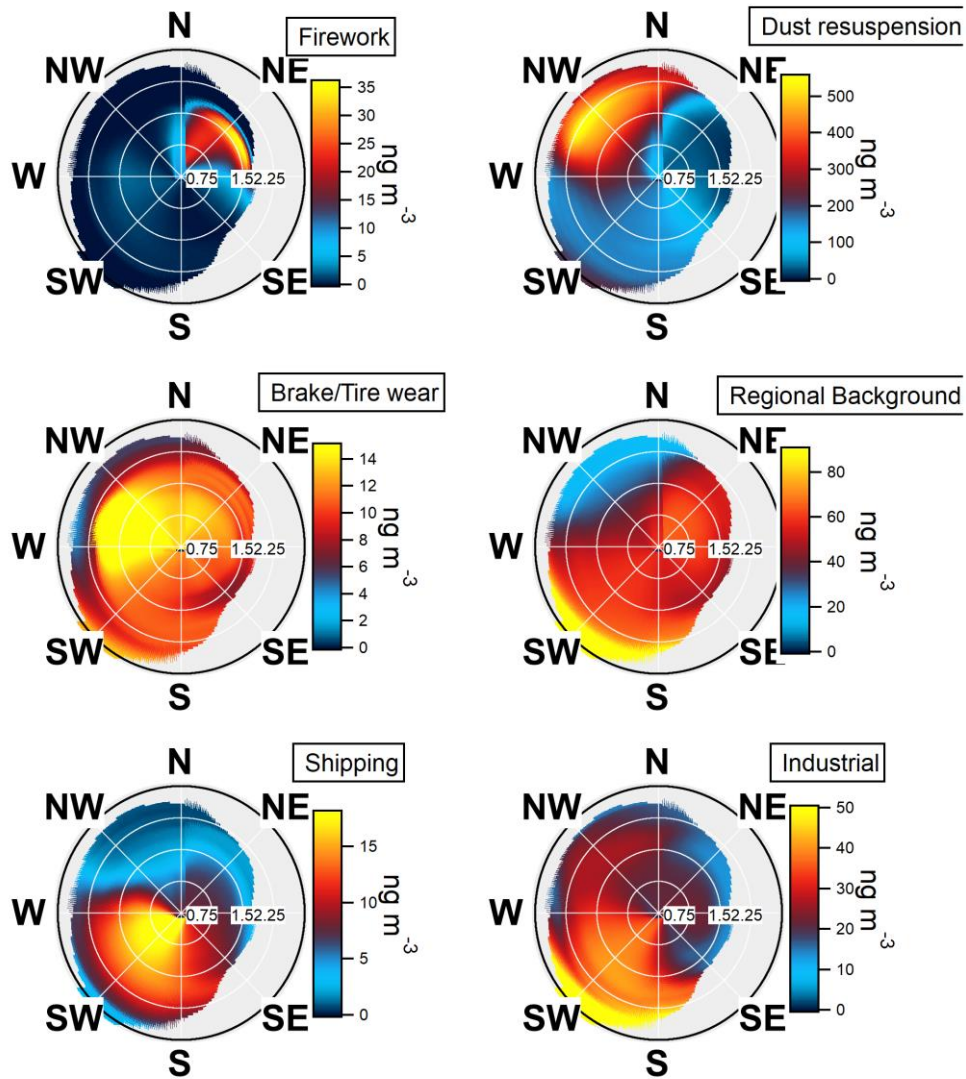
245



246

247 **Figure S8. (a)** Pie chart contributions and **(b)** average diurnal profiles of factors from the $\text{PMF}_{\text{metals}}$
 248 analysis. For the diurnal plots the red dots correspond to the mean, the bands are the median, the bottom
 249 and top of the boxes represent the 25th and 75th percentile respectively, and the ends of the whiskers are
 250 for the 10th and 90th percentiles.

251



252

253 **Figure S9.** NWR plots for the different factors from the PMF_{metals} analysis.

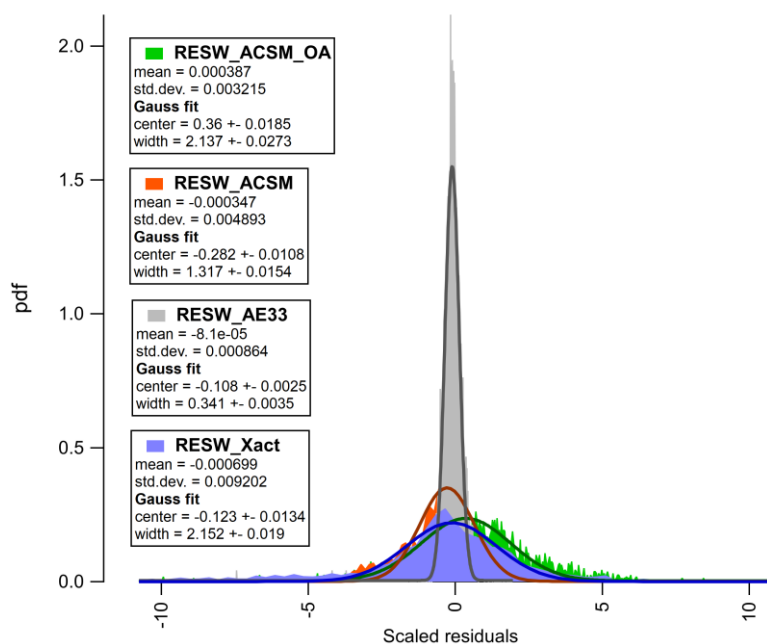
254

255 **Sect. S3: C-value weighting**

256 The instrument weight was controlled by applying a scaling factor (i.e. C-value) to the uncertainties of
 257 each group of components (Slowik et al., 2010):

$$258 (\sigma'_{i,j})_s = \frac{(\sigma_{i,j})_s}{C_s} \quad (S10)$$

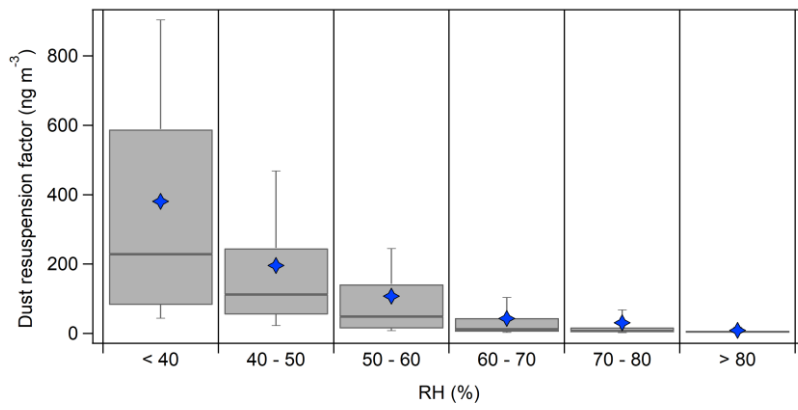
259 σ represents the uncertainties, C the scaling value applied to the s datasets. Here we distinguished the
 260 PMF_{organics} (ACSM_OA), PMF_{metals} (Xact), ACSM inorganics (ACSM) and BC (AE33) datasets. A well
 261 balanced solution should show magnitude of scaled residuals independent from the instrument. Since
 262 their scaled residuals were rather in the same range, a C-value of 1 was chosen for ACSM_OA, Xact and
 263 ACSM datasets and resulted in unweighted results. However, we applied a C-value of 5 to the AE33
 264 dataset, meaning that dataset of BC concentrations were upweighted. The overlapping of scaled
 265 residuals from the different instrument datasets is shown in Figure .



266
 267 **Figure S10.** Probability density function of scaled residuals for the standalone ACSM_OA, ACSM, AE33
 268 and Xact datasets.

269

270



271

272 **Figure S11.** Box plots of dust resuspension factor concentrations for different relative humidity (RH)
 273 bins in %. The concentrations are enhanced under low RH conditions. The blue diamonds are the mean,
 274 the bars inside the boxes the median, the bottom and top of the boxes are the 25th and 75th percentile,
 275 respectively, and the ends of the whiskers are the 10th and 90th percentiles.

276

277

278

279 **Sect. S4: Factors identification and rotational ambiguity exploration for PMF_{PM1}**

280 Seed runs between 1 and 12 factors were examined. The factors interpretability was based on profiles
 281 consistency and our expectations from the factors composition. The summarizes the occurrence of 8
 282 well-identified factors in all runs between 5 and 12 factors. The choice of a 8-factors solution is supported
 283 also by mathematical diagnostics ($\Delta Q/Q_{exp}$, mass reconstruction, ΔUEV – not presented here) which
 284 showed that realistic solutions can be found up to 5 factors. While some factors are easily resolved in
 285 most of the solutions (e.g. dust resuspension) some others are retrieved from an elevated number of
 286 factor (e.g. shipping and cooking are found in up to 9 factors-solution).

287 Therefore, the solution was constrained using base case profiles (Table). The biomass burning, cooking
 288 and industrial factors were constrained as they presented unstable profiles across the different runs.
 289 Constraining the industrial factor allow an improved separation of the shipping factor (see the
 290 discussion below).

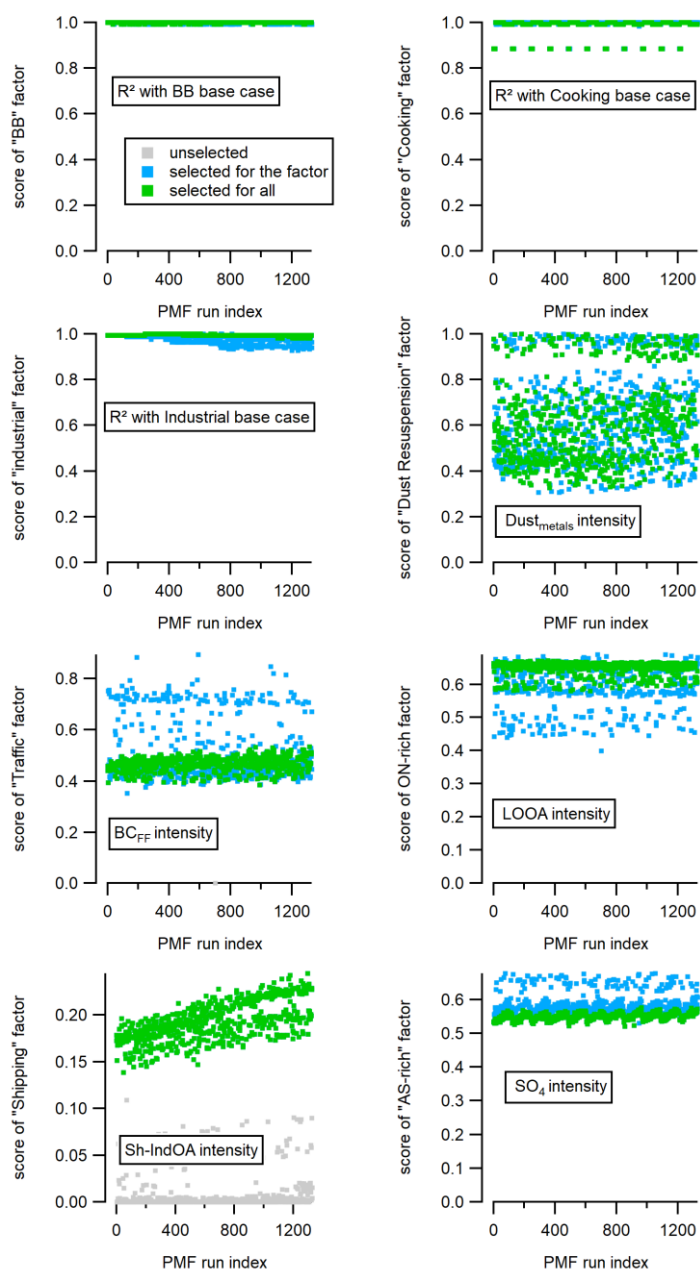
291

	5F	6F	7F	8F	9F	10F	11F	12F
Traffic								
Dust								
AS-rich								
ON-rich								
Industrial								
Shipping								
BB								
Cooking								

292 **Table S4.** Factors identification for the PMF_{PM1} analyses between 5 and 12 factors. The green cells
 293 represent the base case identification for the related factors. The remaining undefined factors for each
 294 solution corresponded to mixed profiles not attributed to a specific source. The red squares are the base
 295 cases used as reference profile constraints.

296 To inspect the best combination of a-values for the profile constraints, we performed a-values sensitivity
 297 analyses by scanning a-values from 0 to 0.5 with increment of 0.05, leading to 1330 outcomes. The
 298 goodness of the solutions was examined with a criteria selection list and the scores are presented in the
 299 Figure . First, the R² correlations between biomass burning, cooking and industrial factors with their
 300 corresponding constraint were monitored. Then, we monitored the intensity of the dominant variable
 301 in the related factor profiles: Dust_{metals} for dust resuspension, BC_{FF} for traffic, LOOA for ON-rich, SO₄²⁻
 302 for AS-rich and Sh-IndOA for shipping. Sh-IndOA was inspected instead of shipping_{metals} to ensure a
 303 clear separation between shipping and industrial factors since Sh-IndOA is assumed to only be
 304 attributed to these two factors. For the first seven criteria, the scores were much higher than the second
 305 highest scores (not displayed in the graph). Therefore, some runs were only discarded based on the

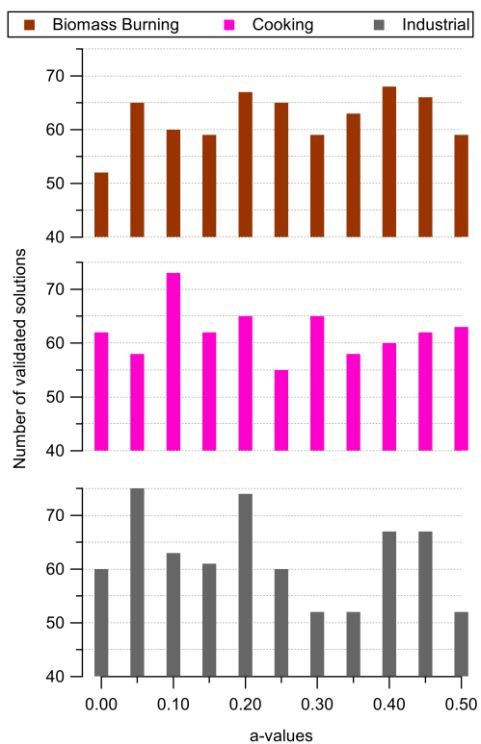
306 shipping criterion as we only selected the runs whose Sh-IndOA intensity was in the same range than
 307 the base case profile from the preliminary analyses. Moreover, the selected runs (green markers in
 308 Figure) showed similar scores intensity for traffic, ON-rich, AS-rich and dust resuspension than those
 309 found in their respective base case profile. In the end, the same criteria list was used for the bootstrap
 310 runs selection.



311
 312 **Figure S12.** Criteria scores for the a-values sensitivity test runs from the PMF_{PM1}. Each graph represents
 313 one criterion per factor. The grey markers are the unselected runs, the blue markers are the selected
 314 runs for the related factor and the green markers are the effectively chosen runs.

315

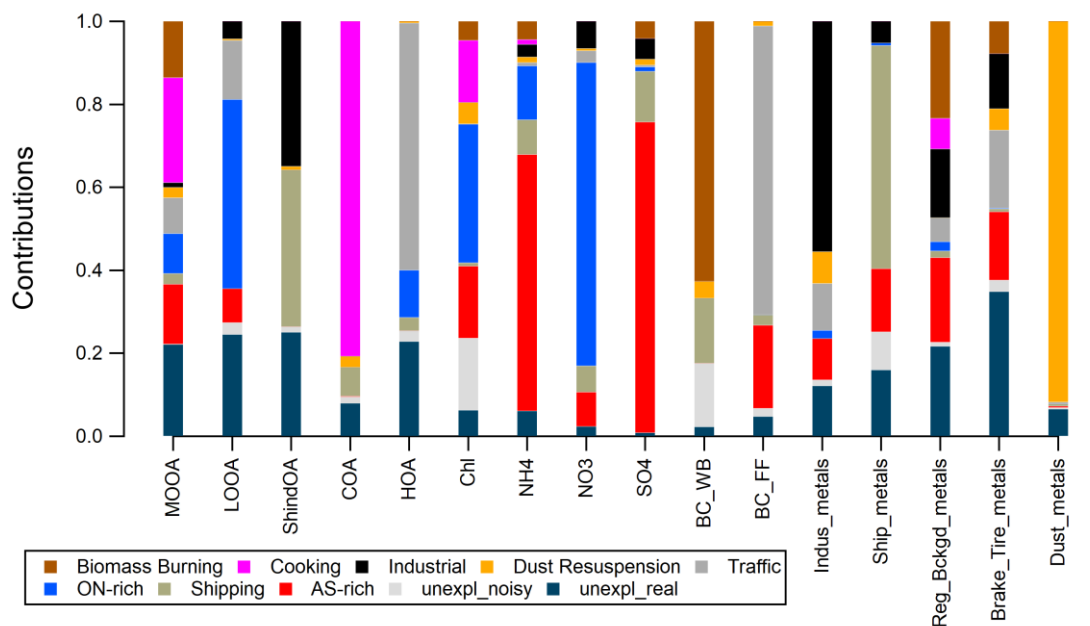
316



317

318 **Figure S13.** Number of accepted solutions based on the PMF_{PM1} criteria list for the different a-values
 319 explored in the sensitivity test. A-values associated to the greatest number of validated solutions were
 320 chosen for the bootstrap PMF runs (i.e. 0.4 for biomass burning, 0.1 for cooking and 0.05 for industrial
 321 constrained profiles).

322



323

324 **Figure S14.** Relative contributions of PM₁ factors profiles and unexplained variations from the PMF_{PM1}
 325 analysis.

326

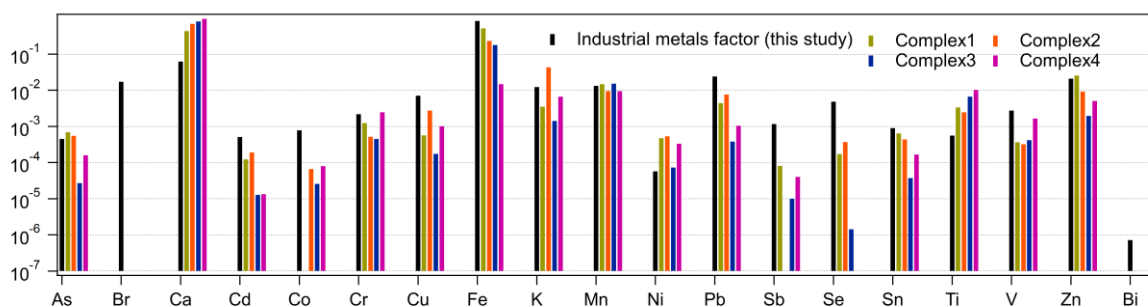
327

328

329

330

331

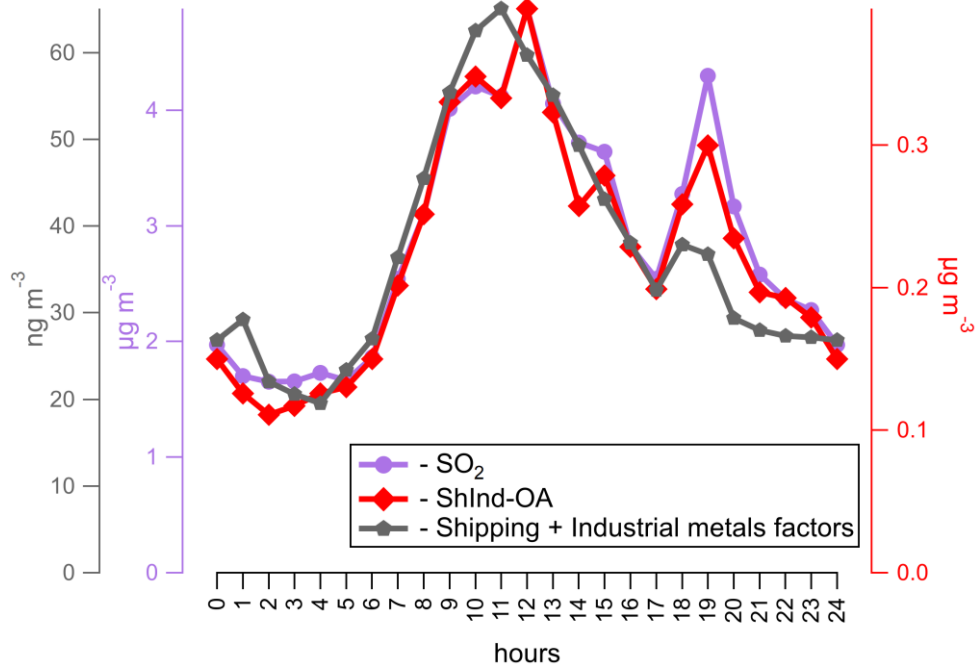


332

333 **Figure S15.** Comparison between the industrial metals profile from our study and ICP-MS profiles for
 334 the PM_{2.5} fraction in the industrial area of Fos-sur-mer (Sylvestre et al., 2017). Complex n°1 is a cast iron
 335 converter complex, complex n°2 is a ore iron converter complex, complex n°3 is a blast furnace slag
 336 storage and complex n°4 is an ore terminal.

337

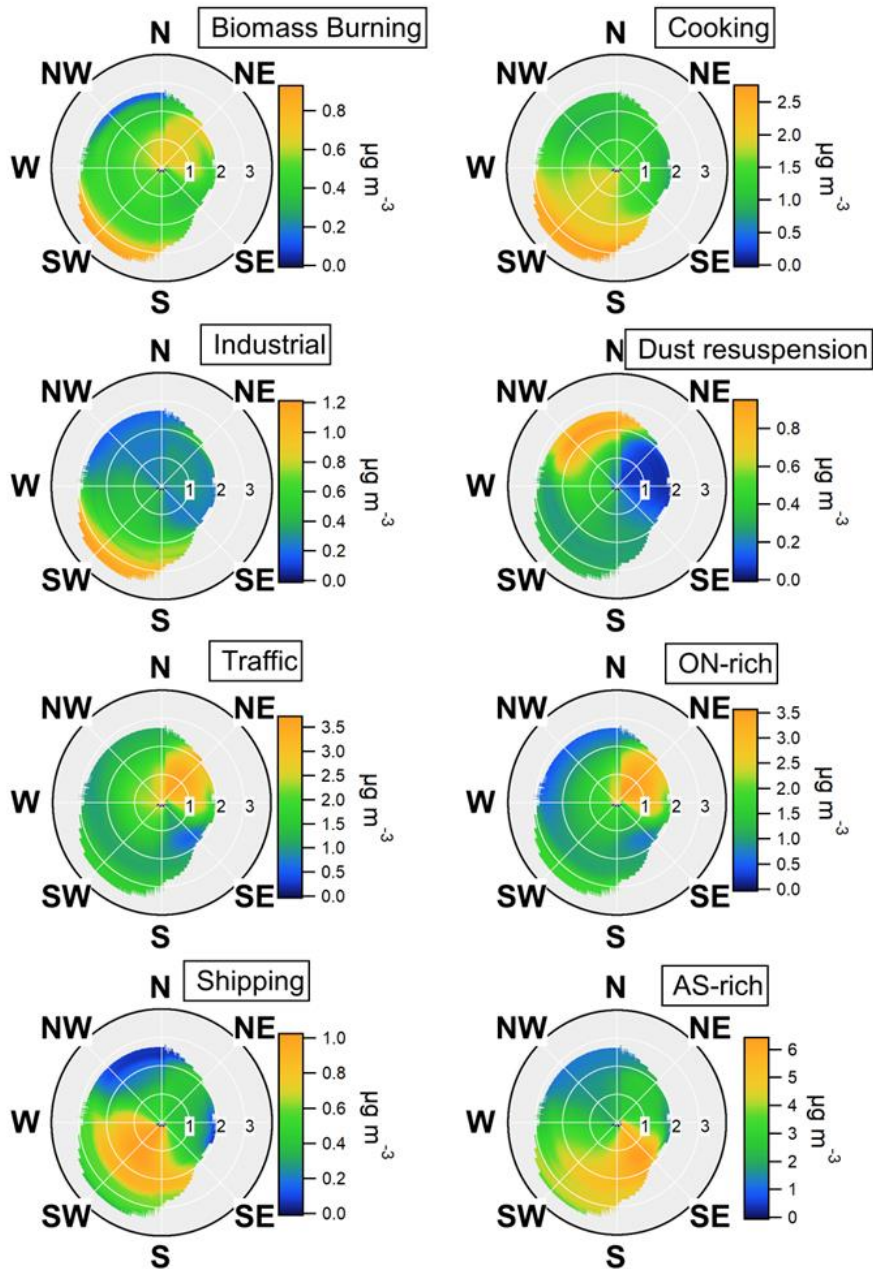
338



339

340 **Figure S16.** Average diurnal profiles for SO₂, Sh-IndOA and the sum of industrial and shipping factors
 341 from the PMF_{metals}.

342



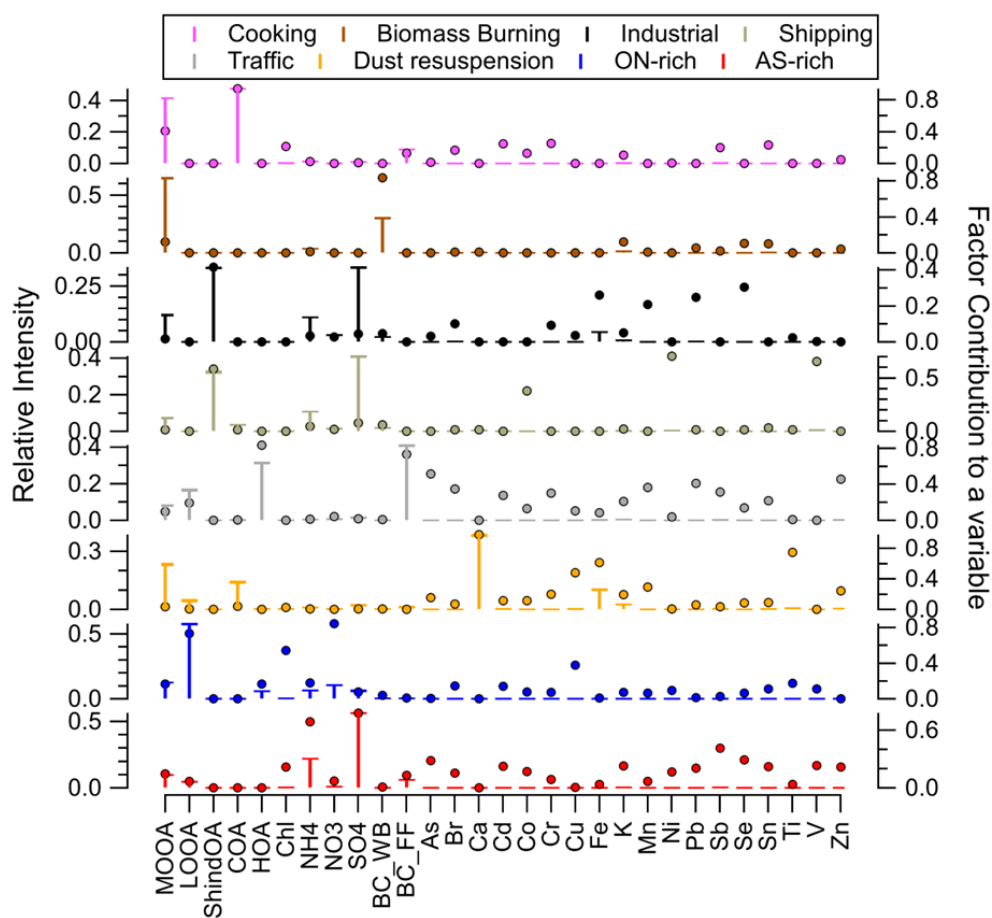
343

344 **Figure S17.** NWR plots for each factor of the PMF_{PM1} analysis.

345

346 **Sect. S5: PMF_{PM1} with OA factors + metals + ions + BC dataset:**

347 Among the 8 identified factors, 4 were not systematically resolved across the several preliminary runs
 348 (cooking, biomass burning, industrial and shipping factors). The solution was constrained using base
 349 case profiles from the 10 factors-solution for industrial, the 11 factors-solution for cooking and shipping,
 350 and the 12 factors-solution for biomass burning. Note that for each run we applied the same C-values
 351 for the instrument weighting than PMF² solution. A bootstrap analysis was performed for 100 runs and
 352 the accepted runs based on the pre-defined list of criteria (the correlation with base case profiles for the
 353 constrained factors and the monitoring of the dominant variable intensity for the unconstrained factors)
 354 were averaged into a definitive solution.



355
 356 **Figure S18.** Average factor profiles for the PMF_{PM1} solution using OA factors, ACSM inorganic species,
 357 BC and metals as inputs. The sticks represent the normalized contribution of the variable to the factor
 358 (left axis) and markers show the normalized factor contribution to each variable (right axis).

359
 360
 361
 362

	R ² with PMF ² factors	Slope with PMF ² factors	Relative contribution (%)
Cooking	0.97	1.18	17.4
Biomass Burning	0.93	0.65	3.3
Industrial	0.95	0.95	2.5
Shipping	0.81	0.52	3.6
Traffic	0.96	1.02	21.5
Dust resuspension	0.99	1.07	2.6
ON-rich	1	1.15	23.1
AS-rich	0.99	0.98	26

363

364 **Table S5.** R² and slope values for the comparison of the PMF_{PM1} (OA factors + metals + ions + BC) factors
365 with PMF² factors. The relative contributions are also represented (in %).

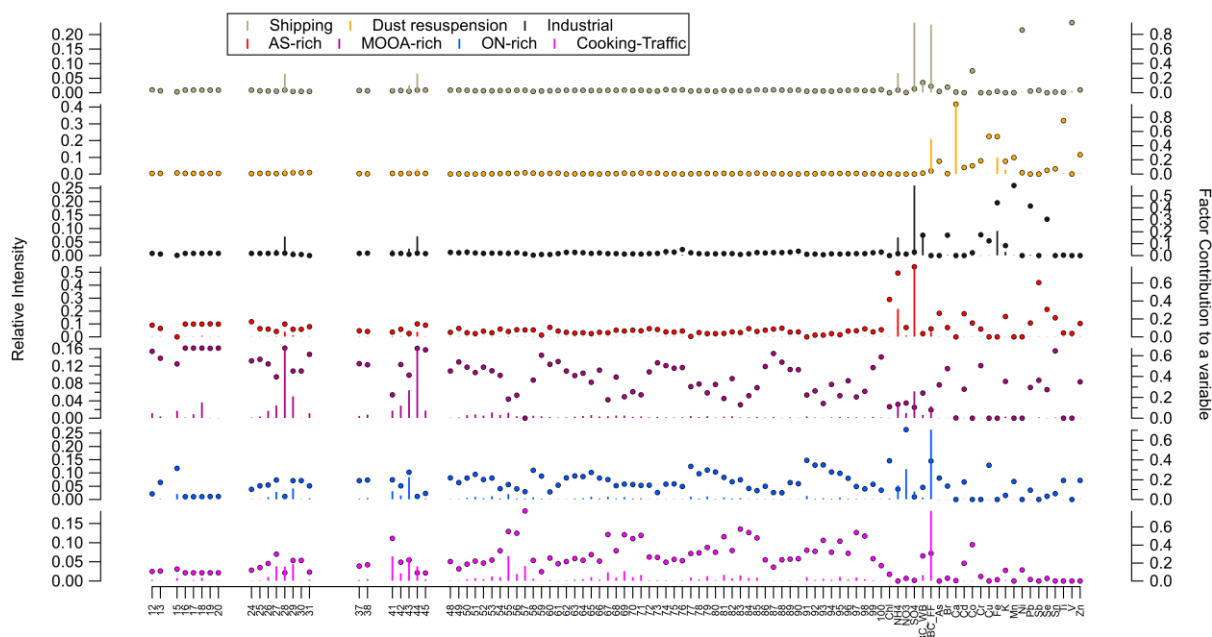
366

367 **Sect. S6: PMF_{PM1} with organic m/z fragments + metals + ions + BC dataset:**

368 This analysis was conducted by merging all datasets prior to analysis, including the organic fragments
369 (from m/z 12 to 100), metals, BC fractions, NO₃⁻, SO₄²⁻, NH₄⁺ and Cl⁻. The data inputs were previously
370 averaged on a similar 1h-time step. This approach could retrieve only 7 sources, and increasing the
371 number of factors did not lead to physically reasonable solutions. The results were compared to the
372 PMF² solution.

373 We successfully identified similar factors than previous methods, with consistent R² correlations:
374 shipping (0.77), dust resuspension (0.99), industrial (0.80) and AS-rich (0.97). However, the
375 identification of the 3 other factors remains challenging. The 5th factor was characterized by an organic
376 m/z spectra showing a high affinity with the MOOA profile (Figure A2) and some elements which were
377 present in the regional background profile from the PMF_{metals} (Br, Sn, K). The 6th factor presented a
378 moderate correlation with the ON-rich factor from PMF² approach (R²= 0.67) but unexpectedly featured
379 a high contribution of BC_{FF} which might be due to some mixing of this factor to traffic.

380 The last factor is interpreted as a result of the mixing of traffic and cooking sources. This lack of clear
381 separation is attributed to the very similar mass spectra profiles of HOA and COA for the organic
382 fraction, which are difficult to deconvolve without applying specific constraints (Chazeau et al., 2022;
383 Chen et al., 2022). The mixing is also evident in the factor's diurnal evolution with unseparated morning
384 and mid-day peaks. Furthermore, the biomass burning source was not resolved in this solution.



385
 386 **Figure S19.** Factor profiles from the PMF solution using organic m/z fragments, ACSM inorganic
 387 species, BC and metals as inputs. The sticks represent the normalized contribution of the variable to the
 388 factor (left axis) and markers show the normalized factor contribution to each variable (right axis).

389
 390 **Associations between both OP and sources of PM**

391 Pearson's correlation coefficients (r) between the source factor contributions identified by the PMF_{PMI}
 392 and both OP assays are presented in Table S6 with the idea to provide a first estimate of the associated
 393 sources with OP. We note that no source strongly correlates alone to both OP assays, but moderate
 394 correlations ($0.3 < r < 0.5$) can be noted for both OP vs. Traffic source (OP_{VAA} : $r=0.40$, $p < 0.001$ - OP_{VDTT} :
 395 $r=0.34$, $p < 0.01$) and Shipping source (OP_{VAA} : $r=0.32$ - OP_{VDTT} : $r=0.30$, $p < 0.01$). OP_{VAA} also correlates
 396 moderately with Industrial source ($r=0.41$, $p < 0.001$) and ON-rich source ($r=0.32$, $p < 0.01$). Finally, OP_{VDTT}
 397 displays a mild correlation with AS-rich source ($r=0.36$, $p < 0.01$), but this correlation might be attributed
 398 to a collinearity with PM mass ($r OP_{VDTT}$ vs $SO_4^{2-}=0.46$, $r OP_{VDTT}$ vs $NH_4^+=0.47$ - $p < 0.001$).

399

	Biomass Burning	Cooking	Industrial	Dust resuspension	Traffic	ON- rich	Shipping	AS- rich
OP_{VAA}	0.15	0.18	0.41***	0.13	0.40***	0.32***	0.32**	0.17
OP_{VDTT}	0.12	-0.02	0.14	0.14	0.34**	0.19	0.30	0.36**

*** $p < 0.001$, ** $p < 0.01$

400 **Table S6.** Pearson's correlation coefficients between OP_{VAA} and OP_{VDTT} to the PM sources identified by
 401 PMF_{PMI} model.

402

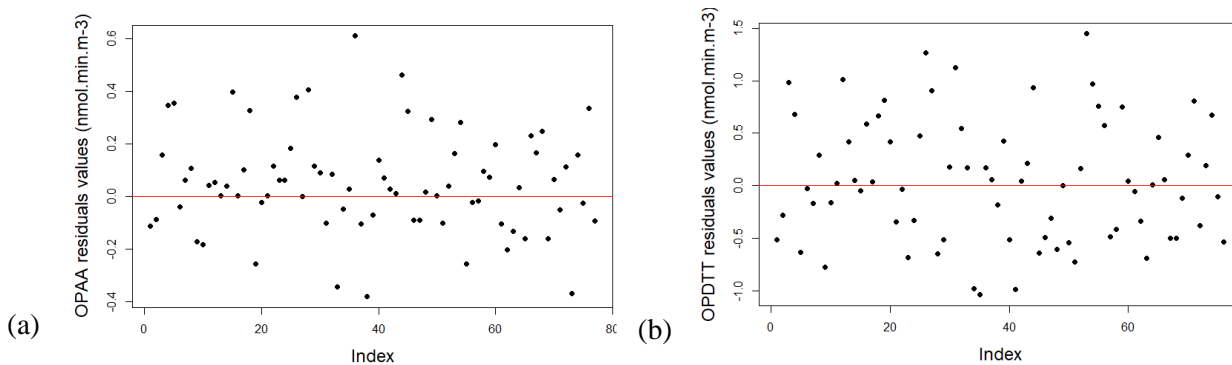


Figure S20. Residuals values of WLS models for **(a)** OP_{AA} and **(b)** OP_{DTT} . An outlier point (19 July 2018 03:00) was withdrawn to ensure homoscedasticity of residuals values.

403

404

405

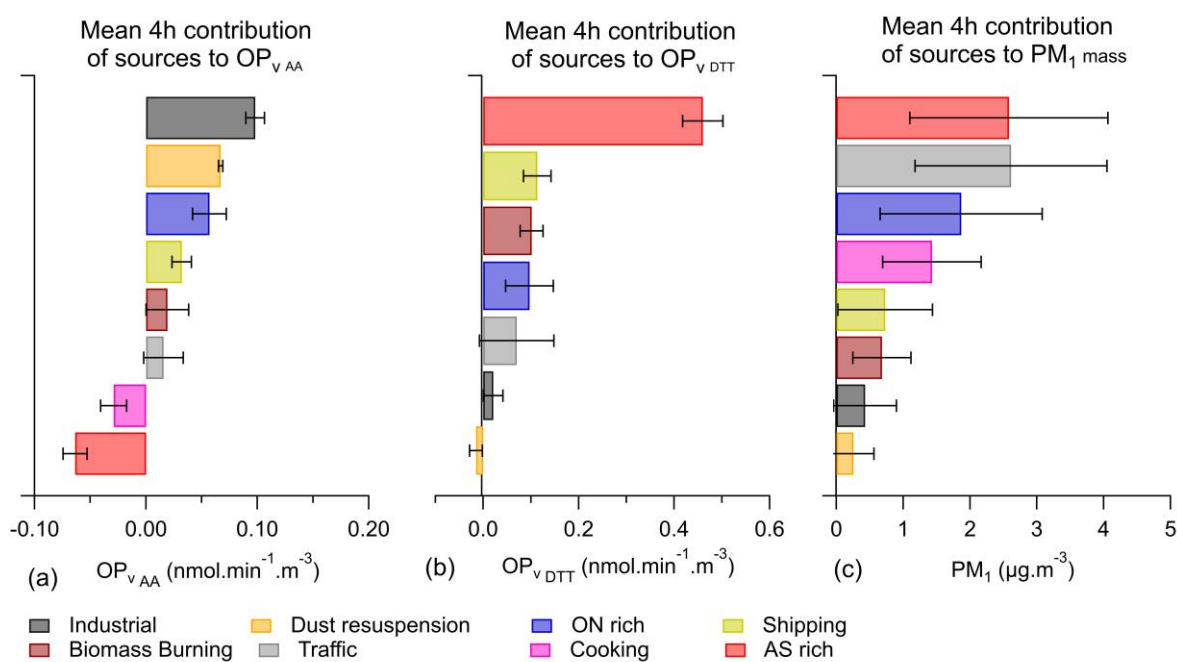


Figure S21. Mean contribution of the sources identified by PMF_{PM1} over the OP sampling campaign ($n = 86$) to **(a)** OP_{AA} , **(b)** OP_{DTT} , **(c)** PM_1 . Error bars represents the standard deviation of the data distribution.

406

407